RSC Advances

PAPER

View Article Online
View Journal | View Issue

Cite this: *RSC Adv.*, 2020, **10**, 25281

Synthesis, structure–fluorescence relationships and density functional theory studies of novel naphthalimide–piperazine–pyridine-based polystyrene sensors for Hg(II) detection†

Yuanyuan Liu,[a] Jingyi Zhang,[a] Tian Feng[a] and Yi Li *[b]

Received 22nd May 2020
Accepted 29th June 2020

DOI: 10.1039/d0ra04557h

rsc.li/rsc-advances

Two novel naphthalimide–piperazine–pyridine-based polystyrene solid-phase fluorescent sensors **PS-NA** and **PS-ND** with different lengths of the linker were synthesized and shown to be able to detect Hg(II) ions. Their structures were characterized by Fourier transform infrared (FTIR) spectroscopy and scanning electron microscopy (SEM) analysis. Fluorescence properties, including response time, pH effects, fluorescence titration, metal ion selectivity and regeneration, were investigated and compared. Sensor **PS-NA** displayed a higher fluorescence response to Hg(II) than **PS-ND**, with a lower detection limit of 1.01 μM. The detection mechanism involving the Hg(II) chelation-induced photo-induced electron transfer (PET) was proposed with the aid of density functional theory (DFT) calculations. Sensors **PS-NA** and **PS-ND** with seven other similar sensors from our previous studies were collected together for thorough structure–fluorescence relationship (SFR) studies. Sensor **PS-NA** being recyclable and environmentally friendly was successfully employed in the fluorescence detection of Hg(II) in real water samples, indicating its good potential in practical application.

1. Introduction

Mercury and its ions as non-biodegradable persistent pollutants are highly cytotoxic and pose a great threat to human health and the natural environment.[1,2] In recent years, more and more Hg(II) fluorescent sensors have been developed due to their simplicity, rapidity, high sensitivity and selectivity.[3–10] However, many of them are difficult to separate from the measured solution, which restricts their reuse on a large scale. Thus, the design of novel economical, environmentally friendly and renewable solid-phase fluorescent sensors has become a hot research topic.

Recently, an indolocarbazole-based macromolecule derived from Suzuki coupling was reported as a solid phase/solution phase sensor for Hg(II).[11] Fmoc solid-phase peptide synthesis (SPPS) was used to give a multifunctional fluorescent peptide sensor for Hg(II) and Cu(II).[12] Both of them have high sensitivity and selectivity, whereas high cost of synthesis and purification may influence their application.

Our groups have made many efforts in the development of novel solid-phase fluorescent sensors for Hg(II) (Fig. 1a–c).[13–15] One common feature of these sensors is that they consist of rhodamine derivative as a fluorescent probe and carboxylated chloroacetylated or chloromethyl polystyrene microspheres as carriers. The polystyrene microspheres exhibit regular shapes, high chemical resistance, and possess a large amount of Cl or carboxyl groups on the surface for further conducting chemical modifications. These chelation-enhanced fluorescence (CHEF) sensors have good anti-interference and recyclable property. However, different size and quantity variance of rhodamines on the surface led to a gap in detection limit.

Naphthalimide and its derivatives with big conjugate system, good rigid coplanarity and large stokes shift, have often been used as fluorophores to construct sensors.[16] In general, most of their sensing mechanisms are based on aggregation-induced emission (AIE),[17–21] photo-induced electron transfer (PET),[22–25] fluorescence resonance energy transfer (FRET)[26–29] and intermolecular charge transfer (ICT).[30,31] If naphthalimides can be modified on polystyrene microspheres, through fine-tuning the existing sensing principles, novel solid-phase sensors with excellent and unique fluorescent performance that traditional chemical sensors do not have may be obtained, which will lead to a promising research area.

[a]*School of Pharmaceutical and Chemical Engineering, ChengXian College, Southeast University, Nanjing 210088, P. R. of China*

[b]*College of Food Science and Light Industry, Nanjing Tech University, Nanjing 211816, P. R. of China. E-mail: liynj2012@njtech.edu.cn*

† Electronic supplementary information (ESI) available: Details for the synthesis of 6-(1,3-dioxo-6-(4-(pyridin-2-ylmethyl)piperazin-1-yl)-1*H*-benzo[*de*]isoquinolin-2(3*H*)-yl)hexanoic acid (**NA-I**), 6-[4-(2-pyridinylmethyl)-1-piperazinyl]-1*H*,3*H*-naphtho[1,8-*cd*]pyran-1,3-dione (**ND-I**) and aminated polystyrene microspheres (**PS-NH$_2$**). See DOI: 10.1039/d0ra04557h

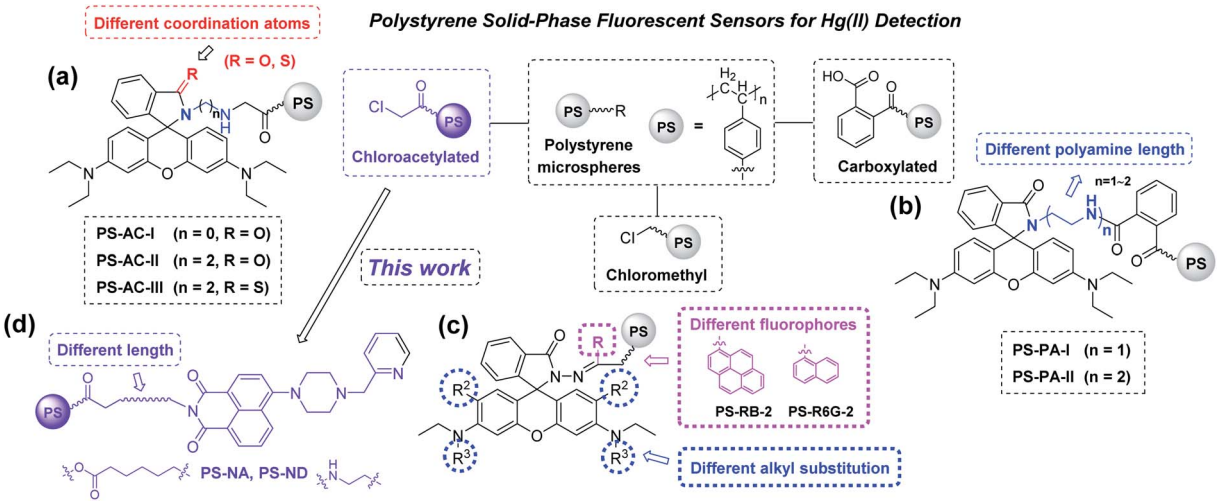

Fig. 1 Design strategy of polystyrene solid-phase fluorescent sensors (a)–(d).

In this paper, two novel naphthalimide–piperazine–pyridine-based polystyrene sensors **PS-NA** and **PS-ND** with different length of linker were designed and synthesized (Fig. 1d). Their fluorescent properties, including response time, pH effects, fluorescence titration, metal ion selectivity and recycling, were investigated. Their structure–fluorescence relationships (SFRs) were compared in detail with our previously reported sensors (Fig. 1a–c) to provide some guidance for further structure modification. The detection mechanism was proposed with the aid of DFT calculations. Sensor **PS-NA** was also employed to fluorescent detection of Hg(II) in real water samples.

2. Experimental

2.1 Materials and reagents

All reagents used were of analytical grade. Nuclear magnetic resonance spectra (NMR) were recorded on a Bruker AV-400 (400 MHz) spectrometer with $CDCl_3$ or DMSO-d_6 as the solvent and TMS as the internal standard. The spectra were reported as δ/ppm downfield from TMS (multiplicity, coupling constant J/Hz, number of protons, assignment). Infrared (IR) spectra were recorded as KBr disks using a Thermo Nicolet 380 FT-IR spectrophotometer. Mass spectra were recorded on a Thermo TSQ Quantum Access MAX mass spectrometer. Scanning electron micrographs were obtained using a JEOL JSM 5900 LV scanning electron microscope. UV-Vis full wavelength scanning was carried out on a Shimadzu UV-2450 spectrophotometer. Fluorescence emission spectra were recorded on a Shimadzu RF-5301PC spectrofluorometer using cuvette (1 cm path length) at r.t. The slit widths were set to 5 nm. Except $Hg(ClO_4)_2\cdot 3H_2O$ was purchased from Alfa Aesar, other salts including $NaNO_3$, KNO_3, $CrCl_3$, $MgCl_2\cdot 6H_2O$, $CaCl_2\cdot 2H_2O$, $FeCl_3\cdot 6H_2O$, $CoCl_2\cdot 6H_2O$, $NiCl_2\cdot 6H_2O$, $Cu(NO_3)_2\cdot 3H_2O$, $CdCl_2$, $AgNO_3$ and $Pb(NO_3)_2$ as well as chloroacetylated polystyrene microspheres (**PS-AC**, 200–300 μm, Cl content: 4.7 mmol g^{-1}) were purchased from Nanjing WANQING chemical Glass ware & Instrument Co., Ltd. The metal ions stock solution (10 mM) was prepared with distilled water and stored in refrigerator at 4 °C for standby. HEPES buffer (pH = 7.2) was used to dilute the stock solution to the required concentration for spectroscopic determination.

2.2 Synthesis of sensors PS-NA and PS-ND

Compound **NA-I** (2 mmol, 0.97 g) and KOH (2 mmol, 0.112 g) were dissolved in methanol (40 mL). The mixture was stirred and refluxed for 1 h, then removed the solvent under reduced pressure to give potassium salt. Chloroacetylated polystyrene microspheres **PS-AC** (170 mg, 0.8 mmol) were swollen in dry DMSO (10 mL) overnight, then potassium salt in DMSO (30 mL) were added. The reaction mixture was stirred at 50 °C for 10 h, then filtered. The microspheres were washed with water and methanol for several times, then dried under vacuum at 30 °C for 24 h to give **PS-NA**.

To a solution of **ND-I** (2.0 mmol, 0.75 g) in ethanol (50 mL) was added aminated polystyrene microspheres **PS-NH$_2$** (0.23 mmol, 85 mg). The mixture was stirred and refluxed for 48 h, then filtered. The microspheres were washed with water and methanol for several times, then dried under vacuum at 30 °C for 24 h to give **PS-ND**.

The loaded amounts of **PS-NA** and **PS-ND** were analyzed by conductometric titration.[32,33] All measurements were repeated thrice. The average Cl contents of **PS-AC** and **PS-NA** were 4.7 mmol g^{-1} and 1.6 mmol g^{-1}, and the average NH_2 contents of **PS-NH$_2$** and **PS-ND** were 2.7 mmol g^{-1} and 1.5 mmol g^{-1}. Therefore, the loaded amounts of **NA-I** and **ND-I** in **PS** were 3.1 mmol g^{-1} and 1.2 mmol g^{-1}, respectively.

2.3 Fluorescence determination

The maximum absorption wavelengths (401 nm for **PS-NA** and 405 nm for **PS-ND**) were determined by UV-Vis full wavelength scanning. Use this wavelength as the excitation wavelength for fluorescence determination.

Sensor **PS-NA** and **PS-ND** (0.01 g) was swollen in acetonitrile (500 μL) overnight, then Hg(II) (1.0 mM, 100 μL) was added. The fluorescence intensity was determined with an excitation

wavelength of 401 nm for **PS-NA** and 405 nm for **PS-ND** every 5 min, to obtain the response time. The effects of pH on their fluorescence intensity was studied in acetonitrile/buffer (1 : 1, v/v) solution. The NaOAc–HOAc buffer (0.1 M, 500 μL) with pH values of 2.0–6.0 and HEPES buffer (0.1 M, 500 μL) with pH values of 7.2–8.0 were selected. For fluorescence titration, Hg(II) (0.1–1 mM, 100 μL) was added to **PS-NA** or **PS-ND** in acetonitrile/HEPES buffer (1 : 1, v/v, pH = 7.2, 900 μL). For metal ions selectivity, 100 μL of Na(I), K(I), Mg(II), Ca(II), Fe(III), Co(II), Ni(II), Cu(II), Cr(III), Cd(II), Ag(I) and Pb(II) (10 mM) or Hg(II) (0.6 mM) was added to **PS-NA** or **PS-ND** in acetonitrile/HEPES buffer (1 : 1, v/v, pH = 7.2, 900 μL), respectively. For anti-interference, Hg(II) (0.6 mM, 100 μL) was added to the above metal ions solution except Hg(II). The fluorescence intensity was determined with an excitation wavelength of 401 nm for **PS-NA** and 405 nm for **PS-ND**. For regeneration, Hg(II) (0.6 mM, 100 μL) was added to **PS-NA** and **PS-ND** in acetonitrile/HEPES buffer (1 : 1, v/v, pH = 7.2, 900 μL). The fluorescence intensity was tested, then Na_2S (10 mM) was added. The fluorescence intensity was tested again in 10 min. The microspheres were filtered, washed with water and acetonitrile for several times, then dried under vacuum at 30 °C for 24 h to recover the free sensors **PS-NA** and **PS-ND**. More than five replicates of each test were carried out.

2.4 Density functional theory (DFT) calculations

The DFT calculations were carried out in the ground state (*in vacuo*) with Gaussian 03 (ref. 34) software by using B3LYP/6-31G** method. The geometrical, electronic and energy parameters were extracted from GuassView 3.0 program based on the optimized structures.

3. Results and discussion

3.1 Synthesis and characterization

Compound **NA-I** was prepared by substitution of 4-bromo-1,8-naphthalic anhydride with 6-aminocaproic acid, piperazine and 2-(chloromethyl)pyridine hydrochloride successively (Scheme 1). Compound **ND-I** was synthesized according to the similar method. Sensors **PS-NA** and **PS-ND** were prepared by using excessive **NA-I** or **ND-I** to react with chloroacetylated **PS-AC** or aminated **PS-NH$_2$** in DMSO or ethanol. Microspheres **PS-NA**, **PS-AC**, **PS-NH$_2$** and **PS-ND** demonstrated good sphericity and monodispersity. The color changed from light yellow or orange to

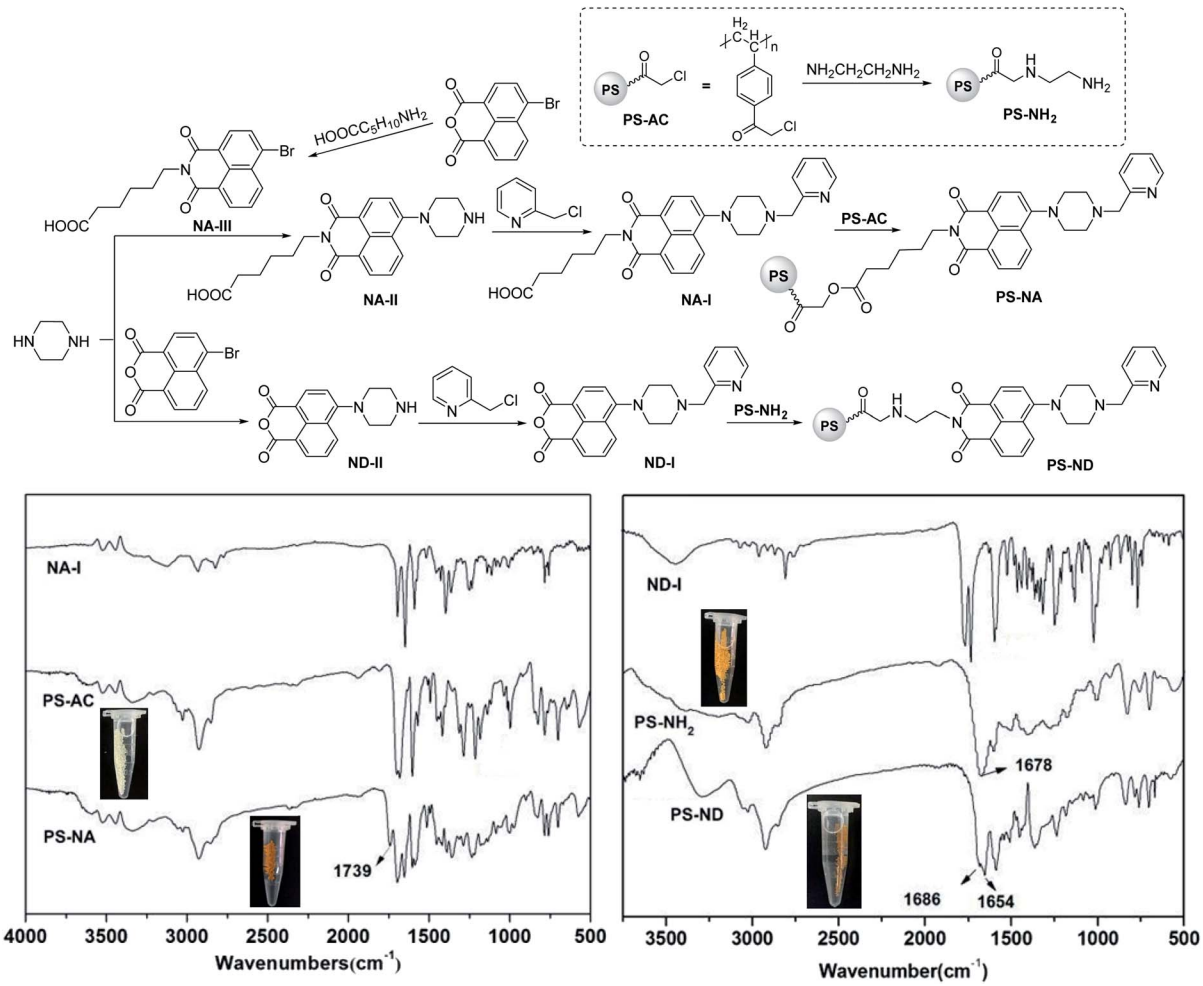

Scheme 1 Synthesis of sensors PS-NA and PS-ND.

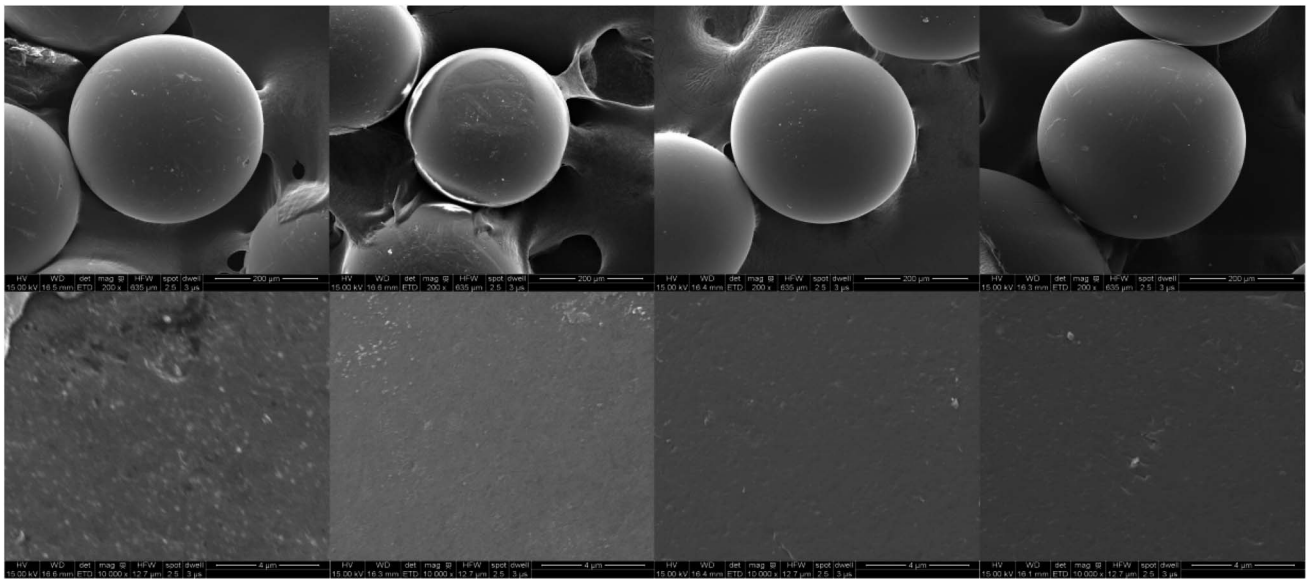

Fig. 2 SEM images of **PS-NA**, **PS-AC**, **PS-NH$_2$** and **PS-ND** (from left to right) (above × 200, below × 10 000).

reddish-brown, indicating **NA-I** and **ND-I** were immobilized on the surface of **PS-AC** and **PS-NH$_2$**, respectively. As shown in FTIR spectra, a new peak appearing at 1739 cm^{-1} in **PS-NA** was attributed to the stretching vibration of the ester C=O. The C–Cl stretching vibration at 995 cm^{-1} was significant weakened in intensity and replaced by the C–O stretching vibrations at 1094 cm^{-1} and 1040 cm^{-1}, indicating that some chloroacetyl groups on the surface of microspheres were substituted. Compared to the C=O stretching vibration of 1678 cm^{-1} in **PS-NH$_2$**, there was another C=O absorption peak of 1654 cm^{-1} in **PS-ND**, indicating the formation of imide.

In order to further illustrate the successful immobilization, a comparison of SEM was undertaken. The SEM allows imaging directly on the surface. As shown in Fig. 2, all the microspheres demonstrated good sphericity and monodispersity, with no significant changes in morphology. The sizes were **PS-AC** < **PS-NA**; **PS-AC** < **PS-NH$_2$** < **PS-ND**. The diameters of **PS-NA** and **PS-ND** increased compared to that of **PS-AC** and **PS-NH$_2$**, and the surface had many recesses. The obvious changes in surface morphology indicated that **NA-I** and **ND-I** were successfully immobilized on the polystyrene microspheres.

3.2 Fluorescence properties

Fluorescence analysis indicated that the recognition between **PS-ND** and Hg(II) was complete in 35 minutes, whereas **PS-NA** responded slightly faster to Hg(II) and its fluorescence intensity was stable in 25 minutes after adding Hg(II). Both of them had potential utility in Hg(II) real-time monitoring. However, the detection of metal ions is easily interfered by protons, so it is necessary to investigate the fluorescence intensity at different pHs. As shown in Fig. 3, the effects of pH on the fluorescence intensity of **PS-NA** and **PS-ND** was basically consistent. When pH value was less than 6, the lower the pH value, the stronger the fluorescence intensity was. The reason might be that with the increase of acidity, the proton could combine with the 1-(pyridin-2-ylmethyl)piperazine recognition group more easily, then produced protonation and blocked the electrons transfer to naphthalene ring, so as to enhance fluorescence. However, **PS-NA** and **PS-ND** produced negligible fluorescence changes at pH values of 6.0–8.0. Therefore, acetonitrile/HEPES buffer (1 : 1, v/v, pH = 7.2) was selected for further spectral analysis.

As shown in Fig. 4, upon the incremental addition of Hg(II), enhanced fluorescence emissions of **PS-NA** and **PS-ND** were observed at 520 nm and 525 nm, respectively. For **PS-ND**, Hg(II) expressed a linear concentration range from 0.01 to 0.1 mM with a correlation coefficient of 0.9887. The detection limit was calculated to 1.98 μM based on 3s/k, where s was the standard deviation and k was the slope of calibration plot.[35,36] Compared to **PS-ND**, **PS-NA** exhibited a higher fluorescence response and

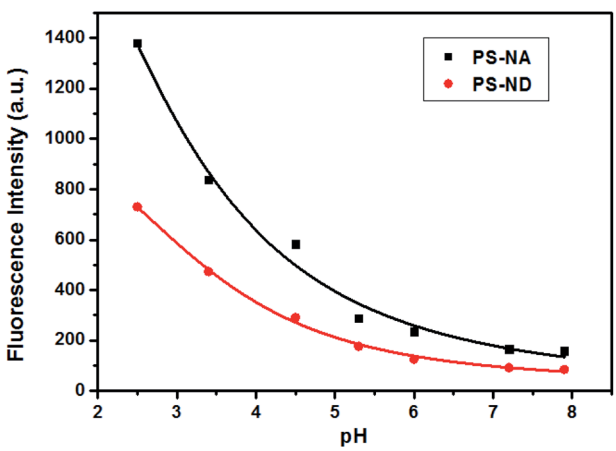

Fig. 3 The effects of pH on the fluorescence intensity of **PS-NA** and **PS-ND** in acetonitrile/buffer solution (1 : 1, v/v) (pH 2.0–6.0: NaOAc–HOAc buffer (0.1 M); pH 7.2–8.0: HEPES buffer (0.1 M)).

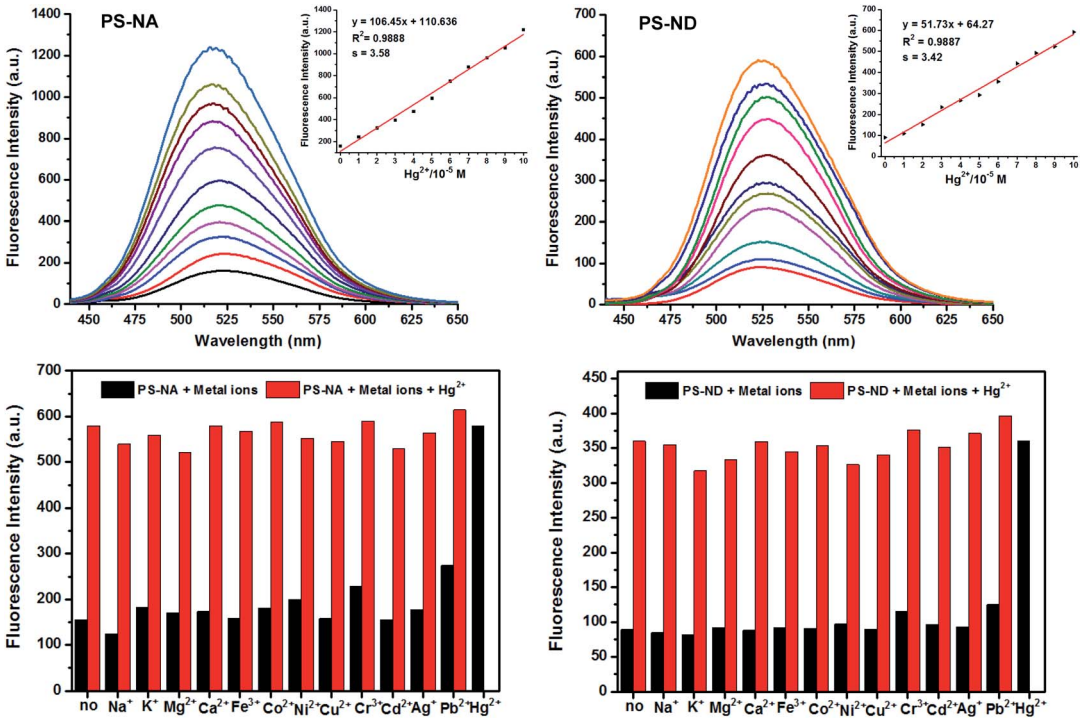

Fig. 4 Fluorescence titration spectra of **PS-NA** and **PS-ND** in acetonitrile/HEPES buffer (1 : 1, v/v, pH = 7.2) upon the incremental addition of Hg(II) as well as the selectivity and anti-interference (**PS-NA**: λ_{ex} = 401 nm; **PS-ND**: λ_{ex} = 405 nm).

a lower detection limit of 1.01 μM. In addition, almost no fluorescence intensity enhancement was detected after adding Na(I), K(I), Mg(II), Ca(II), Fe(III), Co(II), Ni(II), Cu(II), Cd(II) and Ag(I) except with weak response to Cr(III) and Pb(II) (black bars), where the concentration of these metal ions was 10 times higher than Hg(II). However, when Hg(II) was added, significant variation was observed (red bars). Both of them had highly selective to Hg(II) compared to other metal ions and **PS-NA** had a much higher fluorescence response than **PS-ND**.

To verify the regeneration of **PS-NA** and **PS-ND**, sodium sulfide (Na_2S) titrations were carried out. The addition of Na_2S, which had stronger chelation to Hg(II), made the disappearance of fluorescence and regeneration of the free sensors. The most interesting thing was that the sensing behavior was revived by adding Hg(II) again. As shown in Fig. 5, **PS-NA** and **PS-ND** could be reused for more than six times in acetonitrile/HEPES buffer. The slight decrease of fluorescence intensity was due to the loss of some naphthalimides on the surface of microspheres. Cost savings, high selectivity, fluorescence "off-on" response and environment-friendliness by recycling could allow **PS-NA** and **PS-ND** visual recognition of Hg(II) in real sample.

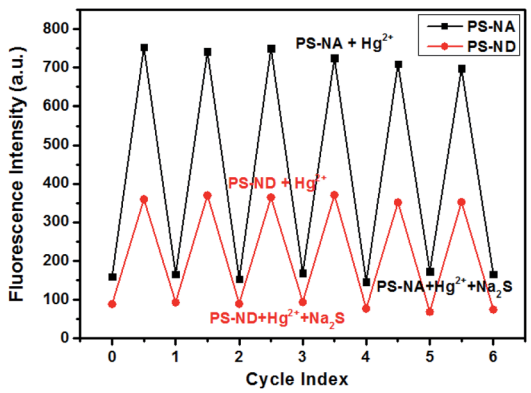

Fig. 5 Fluorescence changes of **PS-NA** and **PS-ND** in acetonitrile/HEPES buffer (1 : 1, v/v, pH = 7.2) after alternate treatment with Hg(II) and Na_2S solution.

3.3 Detection mechanism

When a fluorophore links with an electron-donating group (it generally includes one or more amido N-atoms), the photo-induced electron transfer (PET) will occur.[37–40] In our system, the introduction of the electron-donating recognition group 1-(pyridin-2-ylmethyl)piperazine into the naphthalene ring just forms a push–pull electronic mode with electron-withdrawing imide part. The PET process is easy to occur, thus changing the optical properties of naphthalimide. In order to verify that **PS-NA** and **PS-ND** interact with Hg(II) at the position of 1-(pyridin-2-ylmethyl)piperazine, the ^{1}H NMR spectra of **NA-I**, **ND-I**, **NA-I** + Hg(II) and **ND-I** + Hg(II) were compared together. As shown in Fig. 6A and B, when **NA-I** was combined with Hg(II), both of the methylene peaks in piperazine and 2-methylenepyridine (a_1–c_1) as well as the pyridine peaks (d_1–g_1) moved to the lower field (a_2,–c_2) and (d_2–g_2), respectively. However, the chemical shifts of the hydrogen on naphthalene ring and imide side chain did not shift. Similarly, when **ND-I** was combined with Hg(II), the methylene peaks in piperazine and 2-

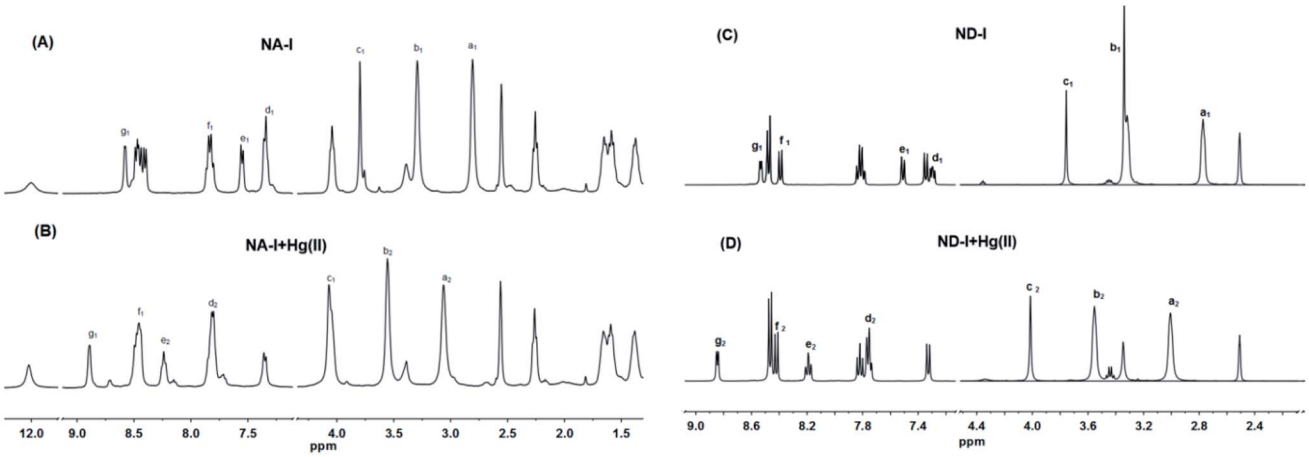

Fig. 6 ^{1}H NMR spectra of **NA-I** (A), **ND-I** (C), **NA-I** + Hg(II) (B) and **ND-I** + Hg(II) (D) in DMSO-d_6.

methylenepyridine (a_1–c_1) shifted to (a_2–c_2), and the hydrogen (d_1–g_1) in pyridine ring shifted to (d_2–g_2) (Fig. 6C and D). Meanwhile, the anhydride was still present, and there was no other group connected to it. It was more powerful to show that Hg(II) was interacted with 1-(pyridin-2-ylmethyl)piperazine but not to the group connected to anhydride.

Based on DFT/B3LYP/6-31G** basis set, the structures of **NA-I**, **ND-I**, **PS-NA** and **PS-ND** were optimized to calculate the HOMO, LUMO and molecular electrostatic potential (MEP). As shown in Fig. 7, compounds **NA-I** and **ND-I** have similar configurations. Both of the piperazine rings adopt envelope conformation and are vertical with the naphthalimide ring. For **NA-I**, the dihedral angle between the piperazine ring and pyridine ring is 111.6°, whereas the corresponding angle in **ND-I** is 112.0°. When they were immobilized on the surface of polystyrene microspheres to form **PS-NA** and **PS-ND**, the configurations in **NA-I** and **ND-I** parts showed almost no change, indicating that **PS-NA** and **PS-ND** should possess similar

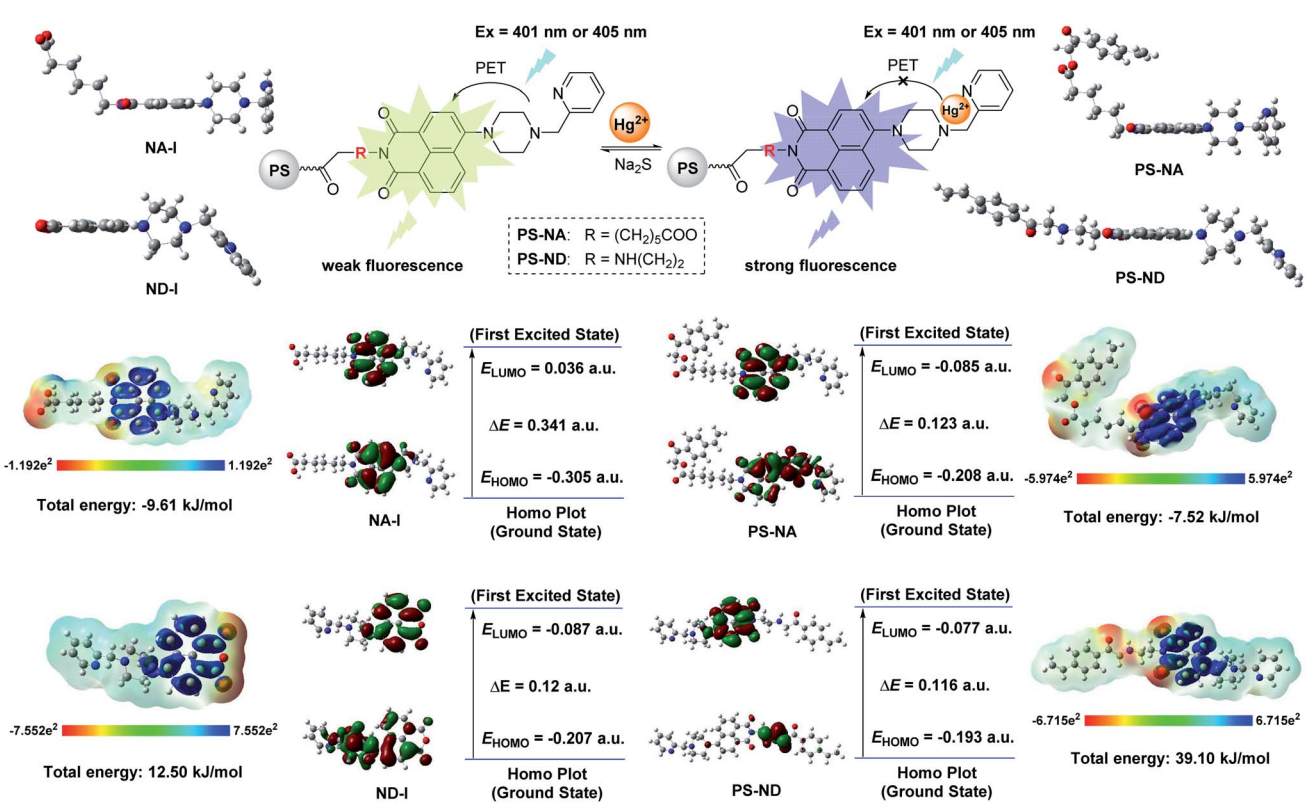

Fig. 7 Detection mechanism of **PS-NA** and **PS-ND** with the aid of DFT calculations (the positive phase and negative phase was symbolized with red and green, respectively).

fluorescent properties with **NA-I** and **ND-I**. In additon, all of them have delocalized π systems. It is easier for the vertical transition of delocalized π electrons from HOMO to LUMO. By comparison of their HOMO–LUMO gaps, the order was: **PS-NA** < **NA-I**; **PS-ND** < **ND-I**. The narrow gap implies a higher reactivity because it is energetically favorable to add electrons to a low-lying LUMO or extract electrons from a high-lying HOMO, and so to form an activated complex in any potential reaction.[41] This might indicate that the electronic transfer in **PS-NA** and **PS-ND** was easier and their chelation with Hg(II) might possess a relatively higher reactivity. In the HOMO of **PS-NA**, the electrons were mainly delocalized on the naphthalimide ring, piperazine ring and the N-atom of pyridine ring. When there was no Hg(II), the electrons in the HOMO of piperazine ring and the N-atom of pyridine ring would enter into the HOMO of naphthalimide, which made the electrons excited to the LUMO of naphthalimide difficult to return to the ground state, and PET process took place, resulting in weak fluorescence. When Hg(II) was added, Hg(II) could coordinate with the N-atom, occupying the HOMO electrons of piperazine ring and the N-atom of pyridine ring, the electron transfer was cut off and the excited electrons of naphthalimide could return to the ground state and prevent the PET process; then, in the LUMO, the electrons were delocalized on the naphthalimide ring, so the fluorescence was greatly enhanced. However, **PS-ND** exhibited quite different HOMO electrons distributions as compared with **PS-NA**. Its electrons were mainly delocalized on the *N*-ethyl side chain as well as the O-atom and N-atom of naphthalimide ring. Although its LUMO electrons distributions, energy gaps and MEP were similar with **PS-NA**, the different degrees of delocalization might affect the PET process, and led to a decrease in fluorescence performance. Furthermore, the immobilization of **NA-I** and **ND-I** on polystyrene microspheres was endothermic reaction, making the total energy of **PS-NA** and **PS-ND** increase, from -9.61 kJ mol^{-1} and 12.50 kJ mol^{-1} to -7.52 kJ mol^{-1} and 39.10 kJ mol^{-1}, respectively. The lower energy (12.50 kJ mol^{-1}) meant a relatively better stability, which made **PS-NA** with a higher fluorescence response to Hg(II). The MEP simultaneously displays the molecular size, shape as well as positive, negative and neutral electrostatic potential regions in terms of color grading. The **PS-NA** and **PS-ND** had similar MEP with **NA-I** and **ND-I**, indicating the immobilization had almost no effect on recognition mechanism.

3.4 Structure–fluorescence relationships (SFRs)

In our previous studies, seven polystyrene sensors **PS-AC-I**, **PS-AC-II**, **PS-AC-III**, **PS-PA-I**, **PS-PA-II**, **PS-RB-2** and **PS-R6G-2** with similar rhodamine fluorophore but different carriers have been prepared (Fig. 1a–c and Table 1). However, their structure–fluorescence relationships (SFRs) have not been discussed together. Here, we wish to report the SFRs of all these nine sensors (including **PS-NA** and **PS-ND** in this paper) from the following three aspects: (i) the effect of different carriers and size; (ii) the effect of different fluorophores and substituents; (iii) the detection limit, mechanism and reused times.

As shown in Table 1, in terms of the rhodamine derivatives as fluorescent probes, **PS-RB-2** and **PS-R6G-2** with smaller size and rhodamine–PAHs fluorophore had relative lower detection limit. The decrease in size would increase the specific surface area and loaded amounts. However, an apparent decrease in fluorescence intensity was presented with the repeat time increase, indicating the rhodamine–PAHs derivatives on the surface of chloromethyl polystyrene microspheres were easily lost. Although chloroacetylated polystyrene microspheres had the bigger size, the higher reactivity of chloracetyl groups on the surface made the immobilization more easily and better, which increased the loaded amounts and led to a similar detection limit (0.439 μM for **PS-AC-I** and 0.483 μM for **PS-AC-II**). The side chain length of polyamines has little effect on their fluorescence properties. Compared to **PS-AC-I** and **PS-AC-II**, **PS-AC-III** had the highest and rapid fluorescence response to Hg(II), with the lowest detection limit of 0.032 μM, which was attributed to the thiophilicity of Hg(II). In terms of the carriers, the carboxylated polystyrene sensors had a relatively higher detection limit (18.4 μM for **PS-PA-I** and 11.0 μM for **PS-PA-II**) than chloroacetylated and chloromethyl sensors, which might because other side reactions occurred during the synthesis of carboxylated microspheres, making the loss of some carboxyl groups and then reducing the loaded amounts. Based on the above analysis and considering reuse times, chloroacetylated polystyrene microspheres were used as carriers in this paper. The naphthalimide derivatives **NA-I** and **ND-I** were synthesized as fluorophores, and the detection mechanism was proposed as Hg(II) chelation-induced photo-induced electron transfer (PET), which was different from our previous work about the Hg(II) chelation-induced ring open of rhodamine. Although the detection

Table 1 Comparison of analytical performance of nine sensors

Carriers	Fluorophore	Sensor	Size (μm)	Detection limit (μM)	Number of recycles
Chloroacetylated polystyrene microspheres	Rhodamine (Fig. 1a)	**PS-AC-I**	200	0.439	≥5
		PS-AC-II	200	0.483	≥5
		PS-AC-III	200	0.032	≥5
Carboxylated polystyrene microspheres	Rhodamine (Fig. 1b)	**PS-PA-I**	200	18.4	≥3
		PS-PA-II	200	11.0	≥3
Chloromethyl polystyrene microspheres	Rhodamine–PAHs (Fig. 1c)	**PS-RB-2**	40	0.065	≥3
		PS-R6G-2	40	0.072	≥3
Chloroacetylated polystyrene microspheres	Naphthalimide (Fig. 1d)	**PS-NA**	200	1.01	≥6
		PS-ND	200	1.98	≥6

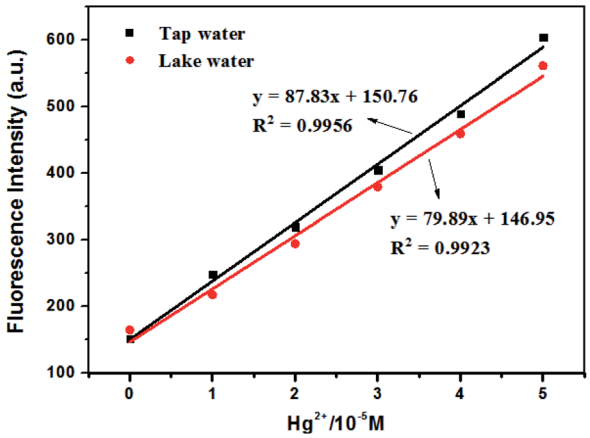

Fig. 8 The relationship between the fluorescence intensity and Hg(II) concentration.

Table 2 Recovery results of PS-NA for spiked Hg(II) in real water samples

Sample	Added (μM)	Detected (μM)	Recovery (%)	Relative error (%)
Tap water	10	9.21	92.1	7.9
	25	23.55	94.2	5.8
	40	38.32	95.8	4.2
Lake water	10	9.15	91.5	8.5
	25	23.47	93.9	6.1
	40	37.88	94.7	5.3

limits of sensors **PS-NA** and **PS-ND** were not the best, the little loss of naphthalimide derivatives on the surface made them have better recovery performance.

3.5 Application

In order to evaluate the actual sample analysis of our solid-phase fluorescence sensors, **PS-NA** with lower detection limit was set as an example to determine the Hg(II) in tap water and lake water. The tap water and lake water were obtained from school and filtered through a 0.22 μm membrane before use.[42] All samples were analyzed by standard addition method and three replicates of each test were carried out. The relationship between the fluorescence intensity and Hg(II) concentration (prepared by tap water or lake water) was shown in Fig. 8. As can be seen in Table 2, the recoveries for tap water and lake water were 92.1% to 95.8% and 91.5% to 94.7%, respectively, with relative errors below 10% in spiked recovery studies. It indicated that the analytical results were within an acceptable range. Thus, the established method with convenient, fast and reliable advantages could be used for the detection of Hg(II) in actual water samples.

4. Conclusions

Two kinds of naphthalimide fluorescent probes **NA-I** and **ND-I** with different linker were immobilized on the chloroacetylated polystyrene microspheres by chemical bonding to form solid-phase fluorescence sensors **PS-NA** and **PS-ND**. Their structures were characterized by FTIR and SEM analysis. Both of them exhibited high selectivity, instantaneous response to Hg(II) and environmental-friendliness by recycling. Compared to **PS-ND**, **PS-NA** displayed a better fluorescence response to Hg(II) with a lower detection limit of 1.01 μM. The detection mechanism involving the Hg(II) chelation-induced photo-induced electron transfer (PET) was proposed with the aid of DFT calculations. The structure–fluorescence relationships (SFRs) of **PS-NA** and **PS-ND** with other seven polystyrene sensors from our previous studies were discussed together. Although the detection limits of **PS-NA** and **PS-ND** were not the best, almost no loss of the naphthalimides on the surface of polystyrene microspheres made them have better recovery performance. Sensor **PS-NA** was successfully applied to monitor Hg(II) in tap water and lake water. High selectivity and instantaneous response to Hg(II), good anti-interference and recyclable property should make **PS-NA** as a potential PET sensor for further monitoring Hg(II) in environmental samples.

Conflicts of interest

There are no conflicts to declare.

Acknowledgements

This work was supported by the Natural Science Foundation of the Higher Education Institutions of Jiangsu Province (17KJB150006), and the Jiangsu Overseas Visiting Scholar Program for University Prominent Young & Middle-aged Teachers and Presidents (2017).

References

1 E. M. Nolan and S. J. Lippard, *Chem. Rev.*, 2008, **108**, 3443–3480.
2 F. Yilmaz, N. Özdemir, A. Demirak and A. L. Tuna, *Food Chem.*, 2007, **100**, 830–835.
3 S. Pan, K. Li, L. Li, M. Li, L. Shi, Y. Liu and X. Yu, *Chem. Commun.*, 2018, **54**, 4955–4958.
4 B. Zhang and L. Guo, *Biosens. Bioelectron.*, 2012, **37**, 112–115.
5 S. Ghosh S, A. S. Alghunaim, M. H. Al-mashhadani, M. P. Krompiec, M. Hallett and L. F. Perepichka, *J. Mater. Chem. C*, 2018, **6**, 3762–3773.
6 E. Bozkurt and H. I. Gul, *Sens. Actuators, B*, 2018, **255**, 814–825.
7 D. Wan, Y. Li and P. Zhu, *Sens. Actuators, B*, 2015, **221**, 1271–1278.
8 Q. Guo, Y. Zhang, Z. Lin, Q. Cao and Y. Chen, *Dyes Pigments*, 2020, **172**, 107872.
9 L. He, H. Tao, S. Koo, G. Chen, A. Sharma, Y. Chen, I. Lim, Q. Cao and J. S. Kim, *ACS Appl. Bio Mater.*, 2018, **1**, 871–878.
10 L. Liu, H. Tao, G. Chen, Y. Chen and Q. Cao, *J. Lumin.*, 2018, **203**, 189–194.
11 M. Vintu, V. K. Rajan, G. Unnikrishnan and K. Muraleedharan, *Eur. Polym. J.*, 2019, **114**, 287–297.

12 X. Pang, L. Wang, L. Gao, H. Feng, J. Kong and L. Li, *Luminescence*, 2019, **34**, 585–594.
13 L. Leng, Y. Li, Y. Liu, F. Li and X. Xiong, *Anal. Lett.*, 2017, **50**, 2944–2958.
14 Y. Liu, Y. Li, L. Zong and J. Zhang, *Chem. Res. Chin. Univ.*, 2019, DOI: 10.1007/s40242-019-9258-3.
15 Y. Li, J. Xiong, S. Li, X. Wen, T. Yu, Y. Lu, X. Xiong, Y. Liu and X. Xiong, *Spectrochim. Acta, Part A*, 2020, **234**, 118277.
16 X. Guo, X. Qian and L. Jia, *J. Am. Chem. Soc.*, 2004, **126**, 2272–2273.
17 H. Liu, S. Wei, H. Qiu, B. Zhan, Q. Liu, W. Lu, J. Zhang, T. Ngai and T. Chen, *Macromol. Rapid Commun.*, 2020, DOI: 10.1002/marc.202000123.
18 J. M. Delente, D. Umadevi, S. Shanmugaraju, O. Kotova, G. W. Watson and T. Gunnlaugsson, *Chem. Commun.*, 2020, **56**, 2562–2565.
19 B. Muzey and A. Naseem, *J. Photochem. Photobiol., A*, 2020, **391**, 112354.
20 C. Balachandra and T. Govindaraju, *J. Org. Chem.*, 2020, **85**, 1525–1536.
21 M. Korzec, S. Kotowicz, R. Rzycka-Korzec, E. Schab-Balcerzak, J. G. Malecki, M. Czichy and M. Lapkowski, *J. Mater. Sci.*, 2020, **55**, 3812–3832.
22 M. Martinez-Calvo, S. A. Bright, E. B. Veale, A. F. Henwood, D. C. Williams and T. Gunnlaugsson, *Front. Chem. Sci. Eng.*, 2020, **14**, 61–75.
23 B. Colasson, A. Credi and B. Ventura, *Chem.–Eur. J.*, 2020, **26**, 534–542.
24 X. Yuan, X. Xu, C. Zhao, F. Zhang, Y. Lu, Y. Shen and C. Wang, *Sens. Actuators, B*, 2017, **253**, 1096–1105.
25 S. Fernandez-Alonso, T. Corrales, J. L. Pablos and F. Catalina, *Sens. Actuators, B*, 2018, **270**, 256–262.
26 J. Qin, Z. Fu, L. Tian and Z. Yang, *Spectrochim. Acta, Part A*, 2020, **229**, 117868.
27 S. Adhikari, S. Ta, A. Ghosh, S. Guria, A. Pal, M. Ahir, A. Adhikary, S. K. Hira, P. P. Manna and D. Das, *J. Photochem. Photobiol., A*, 2019, **372**, 49–58.
28 X. Yuan, T. Leng, Z. Guo, C. Wang, J. Li, W. Yang and W. Zhu, *Dyes Pigments*, 2019, **161**, 403–410.
29 S. Yao and Y. Qian, *Sens. Actuators, B*, 2017, **252**, 877–885.
30 M. S. Refat, L. A. Ismail and A. M. A. Adam, *Spectrochim. Acta, Part A*, 2015, **134**, 288–301.
31 R. Joshi, O. R. Meitei, H. Kumar, M. Jadhao and S. K. Ghosh, *J. Phys. Chem. A*, 2016, **120**, 1000–1011.
32 G. M. Abu El-Reash, R. R. Zaky, M. M. El-Gamil and S. M. El-Emam, *J. Mol. Liq.*, 2019, **288**, 111030.
33 S. H. Hasan, N. S. Othman and K. M. Surchi, *Curr. Anal. Chem.*, 2016, **12**, 330–334.
34 M. J. Frisch, G. W. Trucks, H. B. Schlegel, G. E. Scuseria, M. A. Robb, J. R. Cheeseman and J. M. Millam, *Revision B*. Gaussian. Inc., 2003, Pittsburgh PA.
35 L. N. Neupane, J. M. Kim, C. R. Lohani and K. Lee, *J. Mater. Chem.*, 2012, **22**, 4003–4008.
36 B. Hu, L. Hu, M. Chen and J. Wang, *Biosens. Bioelectron.*, 2013, **49**, 499–505.
37 J. W. Nugent, H. Lee, J. H. Reibenspies, H. Lee and R. D. Hancock, *Polyhedron*, 2017, **130**, 47–57.
38 S. Uchiyama, E. Fukatsu, G. D. McClean and A. Prasanna de Silva, *Angew. Chem. Int. Ed.*, 2016, **55**, 768–771.
39 U. Fegade, S. Attarde and A. Kuwar, *Chem. Phys. Lett.*, 2013, **584**, 165–171.
40 E. B. Veale, J. A. Kitchen and T. Gunnlaugsson, *Supramol. Chem.*, 2013, **25**, 101–108.
41 M. Qiu and K. M. Liew, *J. Phys. Chem. C*, 2012, **116**, 11709–11713.
42 K. Li, W. Jia, D. Han, D. Liang, X. He and G. Chen, *Sens. Actuators, B*, 2017, **246**, 197–201.